Labyrinthine patterns on an inhomogeneous background in a nonlinear optical system

J. Schüttler,* I. Babushkin,† and W. Lange‡
Institut für Angewandte Physik, Westfälische Wilhelms-Universität Münster, Corrensstrasse 2/4, 48149 Münster, Germany
(Received 20 April 2008; published 22 September 2008)

We experimentally show the existence of labyrinthine patterns between spatially modulated steady states in a simple nonlinear optical system consisting of a sodium vapor cell and a single feedback mirror. The inhomogeneity of the steady states leads to a locking phenomenon determining the length scale of the labyrinthine patterns and diminishes their region of existence in favor of localized periodic patterns. Numerical simulations confirm the experimental observations.

DOI: 10.1103/PhysRevA.78.035802 PACS number(s): 42.65.Sf, 42.65.Pc, 05.65.+b, 89.75.Fb

Self-organized labyrinthine patterns have been observed in a variety of pattern-forming systems, including chemical, hydrodynamical, and superconducting ones and others (see [1,2] and references therein). In optics, such states have been experimentally demonstrated only in the degenerate optical parametric oscillator [3], although they are theoretically predicted for some other optical systems, such as vectorial Kerr resonators and in degenerate four-wave mixing [4,5].

A common approach to front dynamics in such systems is to consider a circular "droplet" of one stable state on the background of another one [1,4,7–10], or a straight front between two states [4,6]. In this framework, the modulational instability corresponds to a growth of circular domains driven by the front curvature (or, equivalently, to a "fingering" of a straight front). This is complementary to the formation of solitonlike structures in so far as in both cases a domain shrinks or grows until it ends up in a stable configuration formed by the diffractive locking of the fronts [4,8–11]. Solitons formed on an inhomogeneous background have been considered as well, with an inhomogeneity either inherently belonging to the system (as in transverse photonic crystals [12,13]) or formed due to a self-organization process from an initially homogeneous background [9,8]. Such inhomogeneities play an active role, sufficiently modifying the dynamics [9,12,13]. In particular, in a system analogous to the one considered here they can stabilize otherwise unstable higher-order transverse solitons [9].

In contrast to solitons, the formation of labyrinthine patterns on an inhomogeneous background has not been studied before, to the best of our knowledge. In the present paper we consider a nonlinear optical system with a single feedback mirror, where the steady states are provided by light of opposite circular polarization [9,14]. The pitchfork bifurcation giving rise to these states is followed by a subcritical Turing pattern instability, leading to stationary spatially periodic pattern formation. Here, we consider the Ising fronts connecting two already spatially inhomogeneous states. We demonstrate both experimentally and numerically the possibility of labyrinth formation on such a patterned background. We show that the presence of spatially periodic oscillations in the background leads to the locking of the length scale of the labyrinthine pattern to the characteristic wavelength of the underlying spatial oscillations. In addition, the labyrinth formation does not start directly at the threshold where fronts start to expand, but is intermediated by some parameter region in which the front dynamics is stopped by locking on the underlying oscillations.

The experimental scheme is shown in Fig. 1. The driving light field is a linearly polarized, spatially filtered, and collimated laser beam (beam waist radius $w_0=1.89$ mm) with a frequency some linewidths above the sodium D_1 line. The beam is injected into a heated cell containing sodium vapor in a nitrogen buffer gas atmosphere. The cell is placed in the center of three orthogonal pairs of Helmholtz coils, which compensate the earth's magnetic field and create a dc magnetic field **B** of up to about 25 μT with arbitrary spatial direction.

The feedback loop consists of a planar mirror ($R=0.99$) at a distance d behind the medium and a $\lambda/8$ retardation plate, which represents a modification with respect to the standard scheme [14]. Its slow principal axis is oriented parallel to the direction of polarization of the input beam. The portion of light transmitted by the feedback mirror is used for detection. A second $\lambda/8$ plate rotated by $\pi/2$ with respect to the first one reestablishes the polarization state of the light field behind the cell before detection. A linear polarizer ("analyzer") projects the polarization state onto the component parallel to the input polarization. The lens images the exit plane of the sodium cell onto a CCD camera.

Circularly polarized light produces optical pumping between the Zeeman sublevels of the sodium ground state, i.e., it induces a nonzero "orientation" of the vapor, whose sign

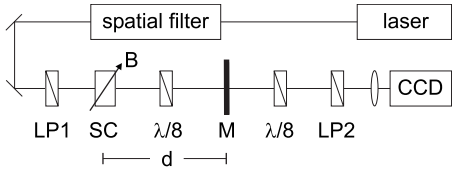

FIG. 1. Schematic experimental setup. LP1 and LP2, linear polarizers; SC, sodium cell; $\lambda/8$, phase retardation plates; M, feedback mirror; CCD, charge coupled device camera.

*Present address: Fraunhofer-Institut für Lasertechnik, Steinbachstrasse 15, 52074 Aachen, Germany. jens.schuettler@uni-muenster.de
†Present address: Max Born Institute A3, Max-Born-Strasse 2a, 12489 Berlin, Germany. ibabush@mbi-berlin.de
‡w.lange@uni-muenster.de

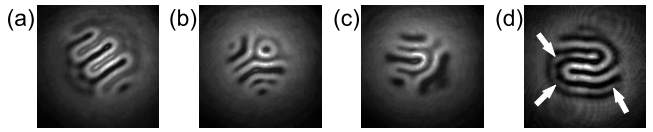

FIG. 2. Examples of labyrinthine patterns observed in the experiment at various parameters. Fronts between the different polarization states appear as bright lines. The slightly darker line marked by arrows in (d) stems from an intermediate spatial modulation (see text).

depends on the helicity of the light. For a linearly polarized input no net pumping should occur. However, in zero magnetic field the system shows spontaneous symmetry breaking between two equivalent spatially homogeneous elliptically polarized states of opposite helicity at a critical pump rate [14,15]. One state is connected with a positive orientation of the medium and a positive rotation of the main axis of polarization, and the other one has a negative orientation and polarization rotation (referred to as "up" and "down" states in the following). This symmetry breaking is a result of a (supercritical) pitchfork bifurcation. At much higher pump levels both of these homogeneous branches become unstable against a modulational instability. Both pattern formation and the existence of polarization domain walls have been demonstrated before [14].

Above the threshold of the modulational instability, complex patterns in the polarization state—like those shown in Fig. 2—are observed. These structures appear spontaneously in switch-on experiments and consist of complex-shaped domains of the up and down states, which are connected by fronts. A comparison with numerical simulations (see below) with plane wave input rather than a Gaussian beam reveals that the observed structures are small portions of extended labyrinthine patterns, limited by the finite size of the beam.

These patterns are only observed with $|\mathbf{B}|=0$ or purely transverse or longitudinal magnetic fields. The threshold is lowest (laser power of the input beam about 250 mW) for a purely transverse magnetic field of 2–3 μT. It should be noted that the pitchfork bifurcation is subcritical under these conditions. For an oblique field, the original pitchfork bifurcation becomes asymmetric and one of the polarization states is preferred. In this case, the whole beam rapidly switches to the preferred polarization state.

The fronts are arranged at discrete distances, which depend on the mirror distance d (roughly proportional to $\sqrt{d}$). For $d=120$ mm, the minimum pitch is 0.35 mm, which is slightly larger than the typical length scale of the (hexagonal) modulational instability mentioned above. Between two fronts, intermediate spatial oscillations around the up or down state without a zero crossing of the orientation are possible [Fig. 2(d); see also Fig. 3]. These oscillations exhibit the length scale of the hexagonal pattern. Depending on the number of intermediate oscillations between two fronts, their distance can have only a few discrete values. A similar behavior is known from a family of transverse solitons observed in the same experimental system [9]. The observed structures change their shape very slowly compared to the intrinsic time scales of the system.

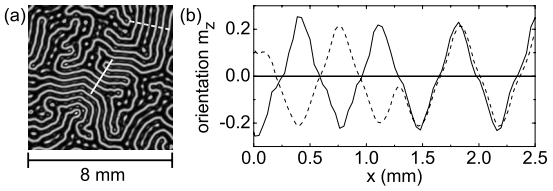

FIG. 3. Spatial length scales in numerical simulations. (a) Light intensity distribution behind LP2. (b) Corresponding orientation distribution along the paths marked solid and dashed in (a). Parameters: $d=120$ mm, $P_0=1.2\times10^5$ s^{-1}, $\mathbf{\Omega}=\mathbf{0}$, $\gamma=1.5$ s^{-1}, and $D=268$ mm^2/s.

The theoretical description of the system is based on a well-established microscopic model (see [16] and references therein). Under the conditions of the experiment, the sodium D_1 line can be modeled as a $J=1/2\rightarrow J'=1/2$ transition with the population of the excited state being negligible. The σ_+ component of the light field brings atoms from the $M=-1/2$ Zeeman substate to the $M=+1/2$ substate with the rate P_+, while the σ_- component works into the opposite direction with the rate P_-. The resulting orientation corresponds to the presence of a longitudinal component m_z of the (normalized) magnetization $\mathbf{m}$. If there is a transverse component B_x of the magnetic field, the other components of $\mathbf{m}$ also come into play. The behavior of $\mathbf{m}$ is described by

$$\partial_t \mathbf{m} = D\Delta_\perp \mathbf{m} - (\gamma + P_S)\mathbf{m} + \mathbf{\Omega}\times\mathbf{m} + P_D\hat{\mathbf{e}}_z, \qquad (1)$$

where γ is the relaxation rate of the orientation, D is the diffusion constant, $\Delta_\perp$ denotes the transverse Laplace operator, and $P_D=P_+-P_-$ and $P_S=P_++P_-$ describe the pumping process. Ω_x is the Larmor frequency produced by B_x, $\Omega_y=0$, and Ω_z is the Larmor frequency produced by B_z and a light shift term [17]. Obviously the pump rates P_+ and P_- are proportional to the local intensities of the polarization components in the superposition of the transmitted and the reflected beams. The transmitted light field is determined by the complex susceptibilities $\chi_\pm$ of the sample which are related to the small signal susceptibility χ_{lin} by $\chi_\pm=\chi_{\text{lin}}(1\mp m_z)$. The polarization components $E_\pm^r$ of the reflected field, which is fed back into the cell, are related to the components $E_\pm^t$ of the transmitted field by

$$\begin{pmatrix} E_+^r \\ E_-^r \end{pmatrix} = \sqrt{\frac{R}{2}} e^{-i(d/k_0)\Delta_\perp} \begin{pmatrix} 1 & -i \\ -i & 1 \end{pmatrix} \begin{pmatrix} E_+^t \\ E_-^t \end{pmatrix}. \qquad (2)$$

Here the exponential stems from the formal integration of the linear wave equation, the matrix describes the action of the $\lambda/8$ retardation plate and R is the reflectivity of the mirror. In the current treatment the variation of the intensity in the interior of the cell used in [16] is neglected. From the analysis of other experiments with similar setup, however, it is expected to have only a marginal influence here.

We performed a linear stability analysis of the transversally infinite system (see below). Moreover, we solved Eqs. (1) and (2) numerically using a split-step algorithm with a fourth-order Runge-Kutta method on a 256×256 point grid. The numerical parameters are chosen to represent the experimental conditions as closely as possible.

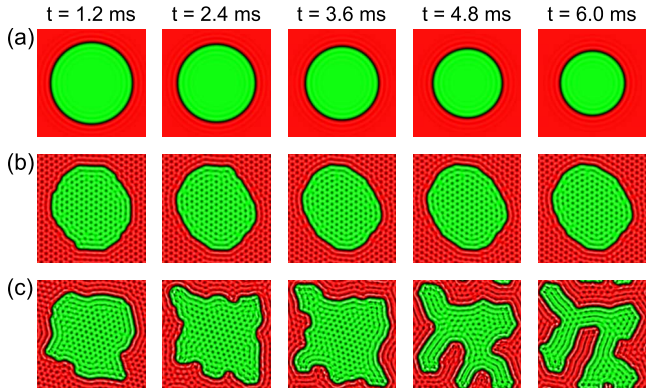

FIG. 4. (Color online) Temporal evolution of circular domains in numerical simulations: P_0=(a) 0.4×10^5, (b) 1.6×10^5, and (c) 2.8×10^5 s^{-1}. Green (within domain), $m_z>0$; red (outside domain), $m_z<0$; black, $m_z=0$. Parameters, see Fig. 3 except d=112 mm.

First, we performed simulations with periodic boundary conditions (plane wave simulations) in order to avoid the influence of the finite size of the input beam. Figure 3(a) shows the calculated light intensity distribution (behind the analyzer) of a labyrinth obtained from a numerical simulation with periodic boundary conditions. Cuts through the corresponding orientation distribution along the paths marked in Fig. 3(a) are shown in Fig. 3(b). The solid line reveals that the orientation is spatially modulated along the cut perpendicular to the local front path with a periodicity length of twice the average front distance. The dashed line shows an example for the intermediate oscillations mentioned above. The length scales found in the simulations agree well with those retrieved from the experiment.

In order to investigate the mechanisms leading to labyrinth formation, plane wave simulations with circular orientation domains as initial conditions were carried out at various pump rates. For pump rates below the threshold for hexagonal pattern formation, the initial domain shrinks with time as shown in the top row of Fig. 4. The contraction of circular domains in this parameter region is known from [9] and can be explained with a curvature-driven dynamics. The middle row of Fig. 4 shows the temporal evolution of the same initial domain at a pump rate slightly above threshold. In this case, the domain keeps its size approximately and only slightly changes the form of its boundary due to an interaction of the front with the beginning patterning of each of the involved states. At a pump rate well above the threshold, the curvature-driven front velocity changes its sign and the front expands in length. Small fluctuations of the local curvature (e.g., induced by the inhomogeneous background) increase at these parameters, leading to labyrinthine patterns as depicted in the bottom row of Fig. 4.

Straight fronts or fronts with a slight transverse modulation show a similar behavior concerning contraction or expansion in length. At low pump rates, a curved portion of a front will move in the direction toward the center of local curvature, which leads to an overall straightening of the front, i.e., the front contracts. At a pump rate above threshold, a front portion will move outward in the direction of the local curvature radius. The front becomes transversely unstable, expands in overall length, and finally forms a labyrinthine pattern.

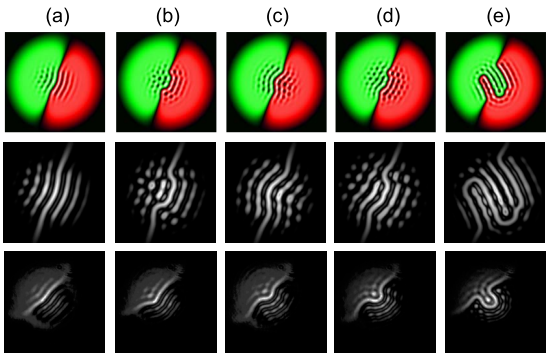

FIG. 5. (Color online) Stable configurations after initial front instability. Top row: orientation distribution from numerical simulations (for the color code, see caption of Fig. 3). Middle row: enlarged clippings of corresponding light intensity. P_0=(a) 0.90×10^5, (b) 1.05×10^5, (c) 1.20×10^5, (d) 1.35×10^5, and (e) 1.50×10^5 s^{-1}. Other parameters, see Fig. 3. Bottom row: Experimental pictures taken at comparable parameters. Laser power: (a) 234, (b) 255, (c) 279, (d) 310, and (e) 326 mW.

The behavior described above can also be reproduced in simulations with a Gaussian pump profile of comparable aspect ratio as in the experiment. It is an obvious consequence of the intensity distribution in a Gaussian beam that far from the beam axis the intensity is low and the fronts are always contracting (straightening), while they can be expanding in the beam center (where the pump rate is sufficiently far above the plane-wave threshold). Typically, after a transient phase, the expansion in the inner part stops due to an interaction of neighboring fronts. Figure 5 shows results of corresponding simulations with various pump rates after reaching such a stable state. In the bottom row experimental pictures taken at comparable parameters are shown. In both cases an increase of the pump rate (input intensity) enlarges the area in which the transverse front instability occurs.

The existence of a transverse modulational instability of the front does not necessarily lead to the formation of labyrinthine patterns. For low values of the transverse magnetic field, the front will initially expand, but then stop due to

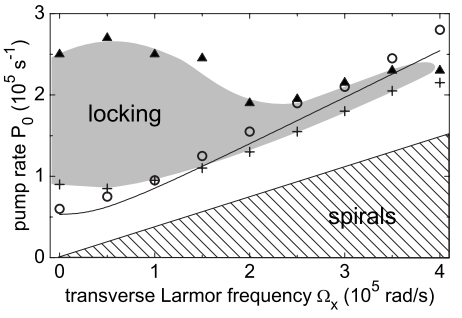

FIG. 6. Instability thresholds obtained from numerical simulations: (○) hexagonal pattern formation, (+) expansion of straight fronts, and (▲) labyrinthine patterns. Shaded: locking regime (see text). Thresholds from linear stability analysis: solid line, hexagonal pattern formation; hatched, Hopf instability leading to spirals. Parameters: see Fig. 3 except d=112 mm, D=200 mm^2/s.

interaction with the patterned underground for a wide range of the input pump rate. Only for pump rates well above the threshold of pattern formation does the front dynamics overcome this "locking" mechanism and lead to the formation of a labyrinth. The locking regime is marked by the shaded region in Fig. 6 and becomes narrower for higher values of the transverse magnetic field. On the other hand, the overall thresholds for pattern formation and the front instability increase with Ω_x. This results in an overall minimum of the threshold of labyrinthine patterns for "medium" transverse fields, which is in good qualitative agreement with our experimental findings.

In the hatched parameter region in Fig. 6, the linear stability analysis mentioned above yields a Hopf instability starting at zero wave number. This instability results in spiral patterns, which can be found in numerical simulations as well as in the experiment. These spirals differ from those reported in [18] in a very similar experimental setup in many details, above all in a significantly different length scale.

We considered the formation of labyrinthine patterns in a nonlinear optical system with feedback that provides two equivalent steady states. For sufficiently high pump rate, the curvature-driven contraction of fronts connecting the steady states is replaced by an expansion, leading to labyrinthine patterns. The system is also subject to Turing pattern formation, causing spatial modulations of the steady states. The labyrinth formation is locked by these modulations, which determine the typical length scale of the labyrinthine pattern. It might be interesting to analyze the relations between the system considered here and optical transverse photonic crystals (TPhCs) [12,13], where the background is also inherently inhomogeneous via a variation of the refractive index and where interaction with the inhomogeneous background leads to a variety of new effects such as discrete diffraction and discrete solitons, stabilization of high-order solitons, and soliton bound states. To our knowledge the formation of labyrinthine patterns has not yet been found in TPhCs.

[1] M. Seul and D. Andelman, Science **267**, 476 (1995).
[2] V. Petrov, Q. Ouyang, and H. L. Swinney, Nature (London) **388**, 655 (1997).
[3] V. B. Taranenko, K. Staliunas, and C. O. Weiss, Phys. Rev. Lett. **81**, 2236 (1998).
[4] R. Gallego, M. San Miguel, and R. Toral, Phys. Rev. E **61**, 2241 (2000).
[5] K. Staliunas and V. J. Sánchez-Morcillo, Phys. Rev. A **57**, 1454 (1998).
[6] K. Staliunas and V. J. Sánchez-Morcillo, Phys. Lett. A **241**, 28 (1998).
[7] D. Gomila, P. Colet, G. L. Oppo, and M. San Miguel, Phys. Rev. Lett. **87**, 194101 (2001).
[8] M. Pesch *et al.*, Phys. Rev. Lett. **99**, 153902 (2007).
[9] M. Pesch, E. Große Westhoff, T. Ackemann, and W. Lange, Phys. Rev. Lett. **95**, 143906 (2005).
[10] M. Tlidi, P. Mandel, and R. Lefever, Phys. Rev. Lett. **73**, 640 (1994).
[11] N. N. Rosanov, *Spatial Hysteresis and Optical Patterns* (Springer, New York, 2002).
[12] D. N. Christodoulides, F. Lederer, and Y. Silberberg, Nature (London) **424**, 817 (2003).
[13] Y. S. Kivshar and G. P. Agrawal, *Optical Solitons: From Fibers to Photonic Crystals* (Academic Press, San Diego, 2003).
[14] E. Große Westhoff *et al.*, J. Opt. B: Quantum Semiclassical Opt. **2**, 386 (2000).
[15] T. Yabuzaki, T. Okamoto, M. Kitano, and T. Ogawa, Phys. Rev. A **29**, 1964 (1984).
[16] A. Aumann, T. Ackemann, E. Große Westhoff, and W. Lange, Phys. Rev. E **66**, 046220 (2002).
[17] M. Möller and W. Lange, Phys. Rev. A **49**, 4161 (1994).
[18] F. Huneus *et al.*, Appl. Phys. B: Lasers Opt. **76**, 191 (2003).